

# Half-Metallicity of LSMO

G. Banach<sup>1,2</sup> and W.M. Temmerman<sup>1</sup>

<sup>1</sup> Daresbury Laboratory, Daresbury, Warrington WA4 4AD, UK

<sup>2</sup> Institute of Low Temperature and Structure Research, Polish Academy of Science, Wroclaw, Poland

(Dated: October 22, 2018)

Self-interaction corrected local spin density approximation calculations were performed for  $\text{La}_{(1-x)}\text{Sr}_x\text{MnO}_3$  (LSMO) ( $0.0 < x < 0.5$ ). The influence and inter-relationship of Sr doping, magnetic structure, O displacements and phase segregation on the Mn charge state were studied. A half-metallic state was obtained for LSMO with manganese configuration  $\text{Mn}^{3+}$ , whilst  $\text{Mn}^{4+}$  gave rise to a metallic state with a negligible spin polarisation at the Fermi level. Elongating the  $\text{MnO}_6$  octahedron led to a static mixed valence  $\text{Mn}^{3+}/\text{Mn}^{4+}$  configuration. In the mixed valence state the total energy was minimized by an ordered array of  $\text{Mn}^{4+}$  and  $\text{Mn}^{3+}$   $\text{MnO}_2$  planes which showed charge ordered stripes.

PACS numbers: 75.47.-m

## I. INTRODUCTION

The half-metallic properties of  $\text{La}_{(1-x)}\text{Sr}_x\text{MnO}_3$  ( $x=0.3$ ) (LSMO) are of great importance for applications in spintronics. The tunnel magnetoresistance junction of LSMO/SrTiO<sub>3</sub>/LSMO shows magnetoresistance ratio in excess of 1800%<sup>1</sup>. This result, according to Ref. 1, strongly underlines the half-metallic nature of mixed-valence manganites. The electronic properties of LSMO, as described by band theory, are nearly half-metallic<sup>2,3,4,5</sup>, reflecting the so-called transport half-metallic behaviour.<sup>6,7</sup> However the fascinating electronic and magnetic properties of LSMO, including colossal magnetoresistance (CMR), indicate that the electronic structure is more complex than the standard band theory picture (see reviews<sup>8,9</sup>). In particular, the electronic structure is determined by the competition of double exchange and superexchange interactions, charge/orbital ordering instabilities, and strong coupling to the lattice deformations. Local Jahn-Teller effects, such as random Jahn-Teller distortions of the  $\text{MnO}_6$ <sup>10</sup> octahedra, as well as dynamical effects<sup>11</sup>, have recently been invoked to explain the magnetoconductivity and optical conductivity respectively. Despite the numerous studies of the phase diagram of  $\text{LaMnO}_3\text{-SrMnO}_3$  (LMO-SMO) (such as in Refs. 12,13,14), there are still many conflicting interpretations of the role of the Jahn-Teller effect in this material<sup>15,16</sup>, localisation of  $d$  electrons,<sup>17,18</sup> and polarisation of electrons at the Fermi level.<sup>19</sup>

In this paper we discuss issues concerning the charge ordering, and more specifically, the distribution of  $\text{Mn}^{3+}$  and  $\text{Mn}^{4+}$  in LSMO. We use the first principles self-interaction corrected local spin density (SIC-LSD) approximation.<sup>20</sup> This method can determine the number of valence band states. Hence, it can differentiate between Mn contributing three states ( $\text{Mn}^{3+}$ ) to the valence band with the remaining four Mn states ( $3t_{2g}$  and  $1e_g$ ) localised well below the valence band, and Mn contributing four states ( $\text{Mn}^{4+}$ ) to the valence band, with the remaining three Mn states ( $3t_{2g}$ ) localised below the valence band. This method was successfully applied to the study of orbital order in  $\text{LaMnO}_3$ .<sup>21</sup>

Calculations with the SIC-LSD as a function of Sr doping are presented in this paper for  $\text{La}_{1-x}\text{Sr}_x\text{MnO}_3$  where  $0.0 \leq x \leq 0.5$ . The Sr doping is modeled with supercells and also with the rigid band approach. In particular we will be concerned with determining the Mn valency as a function of concentration  $x$ . It is found, as expected, that the valency changes as a function of Sr doping from  $\text{Mn}^{3+}$  to  $\text{Mn}^{4+}$ . However, a mixed phase of  $\text{Mn}^{3+}$  and  $\text{Mn}^{4+}$  valencies is found to accompany the valency change. The  $\text{Mn}^{3+}/\text{Mn}^{4+}$  ordering in this mixed phase is consistent with charge ordered stripes. Furthermore it is found that, in the  $\text{Mn}^{4+}$  state and as a function of Sr doping, a change of magnetic structure from ferromagnetic to anti-ferromagnetic takes place. To highlight the effects of Sr doping on the Mn valencies the lattice parameters are kept constant for all concentrations of Sr doping. However, a slightly larger lattice parameter makes the  $\text{Mn}^{3+}$  valency less unfavourable. The structural properties of LSMO show an equally rich variety of charge ordered states. Elongating the  $\text{MnO}_6$  octahedron makes it for the Mn ion more likely to take on the  $\text{Mn}^{3+}$  valency.

The paper is organized as follows. In the next section we introduce the theoretical background of our electronic structure calculations, and in particular, the self-interaction corrected local spin density method. The technical and computational details regarding the application of the SIC-LSD to LSMO are discussed in Section III. In Section IV, we verify that the method works separately for  $\text{LaMnO}_3$  and  $\text{SrMnO}_3$ . Section V discusses the correlation between magnetic structure and charge order in LSMO. The influence of oxygen displacements on the charge order is investigated in Section VI. Section VII presents the results of calculations for various realizations of phase separation and their influence on the charge order. The conclusions of the paper are summarized in Section VIII.

## II. THEORY

The basis of the SIC-LSD formalism is a self-interaction free total energy functional,  $E^{SIC}$ , obtained by subtracting from the LSD total energy functional,  $E^{LSD}$ , a spurious self-interaction of each occupied electron state  $\psi_\alpha$ <sup>22</sup>, namely

$$E^{SIC} = E^{LSD} - \sum_{\alpha}^{occ.} \delta_{\alpha}^{SIC}. \quad (1)$$

Here  $\alpha$  numbers the occupied states and the self-interaction correction for the state  $\alpha$  is

$$\delta_{\alpha}^{SIC} = U[n_{\alpha}] + E_{xc}^{LSD}[\bar{n}_{\alpha}], \quad (2)$$

with  $U[n_{\alpha}]$  being the Hartree energy and  $E_{xc}^{LSD}[\bar{n}_{\alpha}]$  the LSD exchange-correlation energy for the corresponding charge density  $n_{\alpha}$  and spin density  $\bar{n}_{\alpha}$ . The SIC-LSD approach can be viewed as an extension of LSD in the sense that the self-interaction correction is only finite for spatially localised states, while for Bloch-like single-particle states  $E^{SIC}$  is equal to  $E^{LSD}$ . Thus, the LSD minimum is also a local minimum of  $E^{SIC}$ . A question now arises, whether there exist other competitive minima, corresponding to a finite number of localised states, which could benefit from the self-interaction term without loosing too much of the energy associated with band formation. This is often the case for rather well localised electrons like the  $3d$  electrons in transition metal oxides or the  $4f$  electrons in rare earth compounds. It follows from minimisation of Eq. (1) that within the SIC-LSD approach such localised electrons move in a different potential than the delocalized valence electrons which respond to the effective LSD potential. For example, in the case of manganese, three ( $Mn^{4+}$ ) or four ( $Mn^{3+}$ ) Mn  $d$  electrons move in the SIC potential, while all other electrons feel only the effective LSD potential. Thus, by including an explicit energy contribution for an electron to localise, the ab-initio SIC-LSD describes both localised and delocalized electrons on an equal footing, leading to a greatly improved description of static Coulomb correlation effects over the LSD approximation.

In order to make the connection between valence and localisation more explicit it is useful to define the nominal valence as

$$N_{val} = Z - N_{core} - N_{SIC},$$

where  $Z$  is the atomic number (25 for Mn),  $N_{core}$  is the number of core (and semi-core) electrons (18 for Mn), and  $N_{SIC}$  is the number of localised, i.e., self-interaction corrected, states (either three or four for  $Mn^{4+}$  and  $Mn^{3+}$  respectively). Thus, in this formulation the valence is equal to the integer number of electrons available for band formation. To find the valence we assume various atomic configurations, consisting of different numbers of localised states, and minimise the SIC-LSD energy functional of Eq. (1) with respect to the number of localised electrons. The SIC-LSD formalism is governed by the energetics due to the fact that for each orbital the SIC differentiates between the energy gain due to hybridisation of an orbital with the valence bands and the energy gain upon its localisation. Whichever wins determines if the orbital is part of the valence band or not and in this manner also leads to the evaluation of the valence of elements involved. The SIC depends on the choice of orbitals and its value can differ substantially as a result of this. Therefore, one has to be guided by the energetics in defining the most optimally localised orbitals to determine the absolute energy minimum of the SIC-LSD energy functional. The advantage of the SIC-LSD formalism is that for such systems as transition metal oxides or rare earth compounds the lowest energy solution will describe the situation where some single-electron states may not be Bloch-like. For Mn, these would be the Mn  $3d$  states, but not the O  $2p$  states, as trying to localise the latter is energetically unfavourable.

In the present work the SIC-LSD approach, has been implemented<sup>20</sup> within the linear muffin-tin-orbital (LMTO) atomic sphere approximation (ASA) band structure method,<sup>28</sup> in the tight-binding representation<sup>29</sup>.

## III. CALCULATIONAL DETAILS

We performed SIC-LSD calculations for both  $La_{(1-x)}Sr_xMnO_3$  for  $0.0 < x < 0.5$  and SMO. The space group symmetry of the LSMO structure changes, as a function of Sr concentration, from  $Pnma$  (0% of the Sr) to  $R - 3c$  (between 10% and  $\sim 50\%$  of the Sr) and  $P63/mmc$  for SMO. However, for the sake of comparison, we performed calculations using the same cubic crystal structure for all the concentrations. Thus our results for LMO refer to a hypothetical cubic phase. In order to highlight the effect of the electron doping by substituting Sr for La we also kept the lattice parameter constant at 7.32 atomic units (a.u.) - which is the average of the theoretical lattice parameters of ferromagnetic LMO and SMO. The experimental lattice parameter, in going from LMO to SMO, changes by 1%, i.e., from 7.45 to 7.38 a.u..

TABLE I: Energy for different magnetic configurations for cubic  $\text{SrMnO}_3$  referred to the ground state energy. The energy differences are per chemical unit cell and the lattice parameter was taken to be 7.32 a.u.. The  $e_{g(3z^2-r^2)}$  orbital is written as  $1e_g$ . Also displayed are the magnetic moments (MM) for each of the magnetic structures.

	AF-A		AF-G		FM	
	$\Delta E$	MM	$\Delta E$	MM	$\Delta E$	MM
	[mRy]	$[\mu_B]$	[mRy]	$[\mu_B]$	[mRy]	$[\mu_B]$
LSDA	115	2.60	108	2.49	120	2.59
SIC( $3t_{2g}$ )	5	2.74	0	2.79	12	2.68
SIC( $3t_{2g}+1e_g$ )	114	3.44	116	3.47	105	3.44

For the linear muffin-tin basis functions, we used  $6s$ ,  $5p$ ,  $5d$  partial waves for the La and  $5s$ ,  $4p$ ,  $4d$  for the Sr atoms, and treated them as low-waves.<sup>30</sup> Including also  $4f$ -basis functions on the lanthanum, treated as intermediate waves, was of no substantial importance for the final results. On the manganese atoms only  $4s$  and  $3d$  partial waves were treated as low waves, whilst the  $4p$ -waves were treated as intermediate. On the oxygen only  $2s$  and  $2p$  partial waves were treated as low-waves, and  $3d$ -waves as intermediate. The atomic sphere radii were 4.0, 2.3 and 1.8 a.u. for the lanthanum and strontium, manganese and oxygen, respectively. These spheres were chosen to minimise the discontinuity in the Hartree potentials, giving an overlap volume of approximately 8%. No empty spheres were used for the cubic system. Care was taken to ensure that the results were converged with respect to both the size of the screening cluster and the number of  $\mathbf{k}$  points for which the one electron equations were solved. This was imperative to allow comparisons to be made between different magnetic structures, which entailed the use of different unit cells. The screening clusters consisting of 111 atoms for the lanthanum, strontium and manganese sites and 99 atoms for the oxygen atoms were used. The number of  $\mathbf{k}$  points used was 256 in the full Brillouin zone for the paramagnetic/ferromagnetic, G-type and A-type magnetic structures.

To perform calculations for LSMO with  $0 < x \leq 0.5$ , we have utilized the SIC-LSD within the rigid band model and supercell approach. In the rigid band model, the variations in the band filling (reduction by up to 0.5 electrons) and lattice constant were the only variables depicting the change from the cubic  $\text{LaMnO}_3$  to LSMO. Thus taking into consideration the dependence on the lattice constant, we could use the results from rigid band model to describe properties of other perovskites where Sr may be replaced by Ca or Ba. Supercells of the form  $\text{La}_n\text{Sr}_m\text{Mn}_{(n+m)}\text{O}_{3(n+m)}$  (where  $n = 1, \dots, 7$  and  $m=1,2,3$ ) were constructed to describe charge ordering effects due to  $\text{Mn}^{4+}$  occurring in the vicinity of Sr, and  $\text{Mn}^{3+}$  present around La sites.

#### IV. THE END MEMBERS OF PHASE DIAGRAM: LMO AND SMO

We start with the application of the SIC-LSD to the end compounds of LSMO, namely  $\text{LaMnO}_3$  and  $\text{SrMnO}_3$ . Table I summarizes the LSD and SIC-LSD results for SMO for three different magnetic structures, and two Mn valence configurations. As seen in the table, the  $\text{Mn}^{4+}$  configuration in the G-type anti-ferromagnetic (AF-G) structure is the ground state solution. The latter is insulating, with a band gap of 1.08 eV, twice smaller than the measured band gap<sup>17</sup> of 2.3 eV. The ground state configuration corresponds to the localization of the three  $t_{2g}$  electrons. Localizing an extra  $d$  electron, the  $e_g$  one with the symmetry  $d_{3z^2-r^2}$ , giving rise to  $\text{Mn}^{3+}$ , is unfavourable by more than 100 mRy, for all three different magnetic structures. This energy difference between  $\text{Mn}^{4+}$  and  $\text{Mn}^{3+}$  configurations in the ferromagnetic (FM) SMO system decreases from 120 mRy to 93 mRy, when increasing the lattice parameter from 7.2 a.u. (corresponding to the theoretical pseudocubic FM ground state of SMO with  $\text{Mn}^{3+}$ ) to 7.32 a.u.. On the other hand, Table I also shows that only 5 mRy separate the G-type from A-type antiferromagnetic state. This shows that the charge ordering energy in SMO is a much larger energy scale than the magnetic order and that its dependence on the lattice constant is small. The charge transfer of 1.0e and 0.1e respectively from Mn and O atoms to Sr atom hardly changes for the three different magnetic structures. For each magnetic structure the localisation increases the Mn magnetic moment, which, however does not change much between the different magnetic structures.

The FM cubic  $\text{LaMnO}_3$  with the lattice parameter of 7.43 a.u. has the  $\text{Mn}^{3+}$  configuration: 15 mRy separate this ground state from the  $\text{Mn}^{4+}$  excited state. In comparison, for the Jahn-Teller distorted  $\text{LaMnO}_3$  structure, we find 20 mRy energy difference.<sup>21</sup> Reducing the lattice constant by 1.5% to 7.32 a.u., we find that  $\text{LaMnO}_3$  becomes nearly tetravalent and less than 5 mRy separate the  $\text{Mn}^{3+}$  ground state from the  $\text{Mn}^{4+}$  excited state. We find the crossover between trivalent and tetravalent manganese at a volume of elementary cell equal to  $215 \text{ \AA}^3$ . This is close to the expected volume of  $210 \text{ \AA}^3$  from pressure experiments<sup>31</sup>. The charge transfer from Mn and O atoms (respectively 0.9e and 0.2e) gives 1.5 more electrons on the La atom. Thus the charge transfer is similar between SMO and LMO.

TABLE II: Energy for three different magnetic configurations with reference to ground state energy for cubic  $\text{La}_{0.5}\text{Sr}_{0.5}\text{MnO}_3$ . Energy differences are per chemical unit cell and the lattice parameter was taken to be 7.32 a.u..  $\Delta E_{RBM}$  refers to the energy difference from a rigid band model (RBM), whilst  $\Delta E_{SC}$  is the energy difference obtained using a supercell (SC) model. The symbol MM stands for magnetic moment. Four different valence configurations are considered: LSDA,  $\text{Mn}^{4+}$  with the three  $t_{2g}$  electrons localized and the two  $\text{Mn}^{3+}$  valence configurations, localizing each of the  $e_g$  separately.

	$\Delta E_{RBM}$ [mRy]	MM [ $\mu_B$ ]	$\Delta E_{SC}$ [mRy]	MM [ $\mu_B$ ]
AF-A				
LSDA	113	2.67	108	2.77
$\text{SIC}(3t_{2g})$	0	3.04	0	2.99
$\text{SIC}(3t_{2g}+e_{g(3z^2-r^2)})$	63	3.51	63	3.51
$\text{SIC}(3t_{2g}+e_{g(x^2-y^2)})$	48	3.53	47	3.53
AF-G				
LSDA	120	2.62	122	2.56
$\text{SIC}(3t_{2g})$	18	3.02	22	2.89
$\text{SIC}(3t_{2g}+e_{g(3z^2-r^2)})$	64	3.50	62	3.50
$\text{SIC}(3t_{2g}+e_{g(x^2-y^2)})$	64	3.50	63	3.50
FM				
LSDA	111	2.69	113	2.70
$\text{SIC}(3t_{2g})$	4	2.91	6	2.86
$\text{SIC}(3t_{2g}+e_{g(3z^2-r^2)})$	56	3.51	57	3.50
$\text{SIC}(3t_{2g}+e_{g(x^2-y^2)})$	52	3.52	54	3.52

The calculations show that the energy scales between the  $\text{Mn}^{3+}$  and  $\text{Mn}^{4+}$  charge ordered state are much smaller for LMO than for SMO, specifically 20 times smaller. Actually, this is an energy scale comparable to the energy difference between magnetic structures. The competition between these energy scales in the case of Sr doping will be the subject of the next three Sections.

## V. MAGNETIC STRUCTURE AND CHARGE ORDER IN LSMO

In Fig.1 we present the phase diagram of anti-ferromagnetically and ferromagnetically ordered LSMO for Sr concentration between 0.0 and 0.5. For LMO, we obtain a ground state of  $\text{Mn}^{3+}$  valency in an AF-A magnetic structure. In the range of  $x$  up to approximately 0.2 (excluding 0.0), the FM supercell with mixed valence of  $\text{Mn}^{3+}/\text{Mn}^{4+}/\text{Mn}^{3+}$  gives the state with the lowest energy (see also inset of Fig.1). A crossover, as a function of Sr doping, from a FM mixed valence  $\text{Mn}^{3+}/\text{Mn}^{4+}/\text{Mn}^{3+}$  ground state to a FM  $\text{Mn}^{4+}$  ground state occurs around 20% Sr doping. For Sr concentrations between 20% and 35% the ground state has the valency of  $\text{Mn}^{4+}$  in a ferromagnetic structure. For Sr concentrations larger than 40%, the magnetic structure changes to AF-A, but the valency remains  $\text{Mn}^{4+}$ . For  $x$  larger than 0.2, we find that the total energy scales linearly between  $\text{Mn}^{4+}$  and  $\text{Mn}^{3+}$  configurations. We found this by using supercells of up to 8 formula units which allowed us to model different distributions of  $\text{Mn}^{4+}$  and  $\text{Mn}^{3+}$  atoms.

From the top part of Fig.1, we note that for the unfavourable  $\text{Mn}^{3+}$  configuration the energy separation between the two anti-ferromagnetic structures is small. In the  $\text{Mn}^{4+}$  configuration, the energy separating these anti-ferromagnetic structures becomes larger. Obviously, three Mn band electrons are insensitive to the magnetic structure whilst four band electrons, including all  $e_g$  electrons, probe the magnetic structure. From the bottom part of Fig.1, we note that the  $\text{Mn}^{4+}/\text{Mn}^{3+}/\text{Mn}^{4+}$  and the  $\text{Mn}^{4+}/\text{Mn}^{3+}$  configurations are close in energy and also close to the ground state. Increasing the  $\text{Mn}^{3+}$  concentration as realized in the  $\text{Mn}^{3+}/\text{Mn}^{4+}/\text{Mn}^{3+}$  configuration takes the total energy further away from the ground state energy as the hole doping increases through the increase of Sr concentration. Also for a slightly larger lattice constant (7.43 a.u.) the deviation from the ground state energy steadily increases upon hole doping. The  $\text{Mn}^{3+}$  configuration is energetically the most unfavourable. The differences between supercell description and rigid band are small on the energy scale of the separation to the  $\text{Mn}^{4+}$  ground state and the larger the hole doping becomes the more unfavourable the  $\text{Mn}^{3+}$  configuration turns out to be.

The  $\text{La}_{0.5}\text{Sr}_{0.5}\text{MnO}_3$  system was studied using both the rigid band model and  $\text{LaSrMn}_2\text{O}_6$  supercell. From Table II, we note that in the LSD we obtain a FM state in the rigid band model, whilst an AF-A state is obtained in the

supercell approximation. The energy differences between these magnetic structures are 2 and 5 mRy for the rigid band model and supercell, respectively. The SIC-LSD calculations give the same ground state both in the rigid band model and supercell. Similarly to LSD, small energy differences of 4 and 6 mRy separate the AF-A ground state from the FM state in the rigid band model and supercell respectively. Figure 1 also confirms that the rigid band model is an adequate description of the disordered La/Sr system. A comparison is made with supercell calculations of  $\text{La}_n\text{SrMn}_{(n+1)}\text{O}_{3(n+1)}$  with  $n = 1, \dots, 7$ . From energy differences between  $\text{Mn}^{4+}$  and  $\text{Mn}^{3+}$  systems for each  $n$  we deduce an  $\text{Mn}^{3+}$  ground state configuration for  $n$  larger than 9 (for such system as  $\text{La}_{10}\text{SrMn}_{11}\text{O}_{33}$ ) which is in agreement with  $x < 0.1$  from the rigid band model. This shows the close agreement between these calculations.

From Table II, we also note that the energy differences between  $\text{Mn}^{4+}$  and  $\text{Mn}^{3+}$  are more or less constant with respect to the magnetic structure and also with respect to the symmetry of the localized  $e_g$  electron in the  $\text{Mn}^{3+}$  configuration. This energy is approximately 60 mRy. Again the energy differences between magnetic structures are an order of magnitude lower.

The energies in Fig. 1, are closely balanced and the value of the lattice constant will therefore be important. Increasing the lattice constant by 1% to 7.39 a.u., we find that for LMO the ground state remains AF-A with  $\text{Mn}^{3+}$  for Sr concentration  $x$  up to 0.1, and turns into FM with  $\text{Mn}^{4+}$  configuration for  $x$  larger than 0.1. The  $\text{Mn}^{3+}$  configuration has at the same time become slightly less unfavourable. This we note, for example, by comparing the energy difference for  $\text{La}_{0.7}\text{Sr}_{0.3}\text{MnO}_3$  between FM  $\text{Mn}^{4+}$  and  $\text{Mn}^{3+}$  configurations which reduces from 32 mRy at lattice constant 7.32 a.u. to 21 mRy at the 1% increased lattice constant of 7.39 a.u.. For  $\text{La}_{0.5}\text{Sr}_{0.5}\text{MnO}_3$  even the ground state changes from AF-A at the lattice constant of 7.32 a.u. to FM at 7.39 a.u., the energy differences being 4 mRy and -2 mRy respectively. This shows that the combined effect of band filling and the value of the lattice constant gives rise to a rich variation in magnetic structure and charge order.

The spin magnetic moments increase only slightly in comparison with LSD results. For  $\text{La}_{0.7}\text{Sr}_{0.3}\text{MnO}_3$  the Mn spin magnetic moment is  $3.14 \mu_B$  in SIC-LSD and  $3.03 \mu_B$  in LSD and for  $\text{La}_{0.5}\text{Sr}_{0.5}\text{MnO}_3$  these are  $2.91 \mu_B$  and  $2.69 \mu_B$  respectively. The density of states for LSD calculations and the SIC-LSD in  $\text{Mn}^{4+}$  and  $\text{Mn}^{3+}$  configurations are shown in Fig. 2. We clearly see the majority Mn  $t_{2g}$  peak, which occurs in the LSD calculation just below the Fermi level, which moves down in energy below the bottom of the valence band for the calculations for  $\text{Mn}^{4+}$  and  $\text{Mn}^{3+}$  valencies. In the  $\text{Mn}^{4+}$  ground state configuration for  $\text{La}_{0.7}\text{Sr}_{0.3}\text{MnO}_3$  a metallic state is obtained and the electronic structure in the vicinity of the Fermi level is similar to the LSD, i.e., it is also a nearly half-metallic system. However, for the  $\text{Mn}^{3+}$  configuration, we obtain a half-metal with 1.6 eV band gap in the majority spin channel. We will see in the following that the occurrence of a half-metallic density of states is closely associated with the  $\text{Mn}^{3+}$  valency.

The importance of local effects was studied with supercells. From calculations for  $\text{LaSrMn}_2\text{O}_6$  we note that the O atom in SrO layer ( $\text{O}_{Sr}$ ) lost twice as many electrons as the O atom in the LaO layer ( $\text{O}_{La}$ ). This leads to an increased spin moment of  $0.2 \mu_B$  for  $\text{O}_{Sr}$  in comparison with  $0.07 \mu_B$  for  $\text{O}_{La}$ . From calculations for  $\text{La}_2\text{SrMn}_3\text{O}_9$ , we find that Mn sandwiched between two LaO layers loses 0.07 electrons more than Mn between a LaO and SrO layer. However, this increases the magnetic moment for Mn sandwiched between LaO by  $0.04 \mu_B$  only. A similar effect has been noted for calcium perovskites<sup>32</sup>.

## VI. OXYGEN DISPLACEMENTS AND CHARGE ORDER IN LSMO

We investigated the influence, on the Mn valency, of a tetragonal shift of the oxygen atom away from the SrO layer. An upward shift in the  $z$ -direction of 5% of the lattice constant was implemented. We calculated the total energies for a double unit cell, in the FM state, of  $\text{La}_{(1-x)}\text{Sr}_x\text{MnO}_3$  (with  $x=0.3$  and 0.5) of the following configurations: all  $\text{Mn}^{4+}$ , all  $\text{Mn}^{3+}$ , and mixed  $\text{Mn}^{4+}/\text{Mn}^{3+}$  (Fig. 3). For the mixed valence configuration, the  $\text{Mn}^{3+}$  atom is taken to be inside the octahedron which is elongated by the tetragonal shift (see the cell on the right hand side of Fig. 3). In the case of  $\text{La}_{0.5}\text{Sr}_{0.5}\text{MnO}_3$ , we found that increasing the tetragonal shift for the oxygen atom decreases the difference between the energy of the ground state (AF-A with  $\text{Mn}^{4+}$ ) and the energy of the mixed valence  $\text{Mn}^{3+}/\text{Mn}^{4+}$  configuration.

We have calculated a change in the AF  $\text{Mn}^{4+}$  ground state configuration as a function of tetragonal shift of O atom. For  $\text{La}_{0.5}\text{Sr}_{0.5}\text{MnO}_3$  the new mixed valence  $\text{Mn}^{4+}/\text{Mn}^{3+}$  ground state occurs at 4% shift in the rigid band model and a 3% shift in the supercell model. In both models the  $\text{Mn}^{3+}$  configured atom was placed in the elongated  $\text{MnO}_6$  octahedron. Placing the  $\text{Mn}^{4+}$  in the elongated octahedron and the  $\text{Mn}^{3+}$  in the squashed octahedron was the most unfavourable scenario. The crossover to a new ground state also depends on the Sr concentration and for  $\text{La}_{0.7}\text{Sr}_{0.3}\text{MnO}_3$  we find the new ground state already at 1% upward shift of O.

The difference between rigid band model and supercell results for  $\text{La}_{0.5}\text{Sr}_{0.5}\text{MnO}_3$  shows the important role of the local environment, such as presence of Sr atoms, for the electronic properties of this material. Also, the magnetic moment on  $\text{Mn}^{3+}$  increases slightly from  $3.52 \mu_B$  to  $3.63 \mu_B$ , which is connected with 0.1e larger charge transfer from this atom, and decreases from  $2.91 \mu_B$  to  $2.73 \mu_B$  on  $\text{Mn}^{4+}$ . The oxygen atom, shifted in the supercell calculation, has a magnetic moment of  $0.22 \mu_B$ , twice larger than in the undistorted structure.

In the bottom panel of Fig. 3 we present the polarisations of the electrons at the Fermi level. For shifts larger than 3% of the lattice constant the system becomes fully polarised at the Fermi level and we obtain a half-metallic state. In Fig. 4 we show the density of states for mixed valence  $Mn^{4+}/Mn^{3+}$  system without tetragonal shift, mixed valence  $Mn^{4+}/Mn^{3+}$  system with tetragonal shift for oxygen atom (4% of lattice constant) and for AF-A system with  $Mn^{4+}$  configuration. When increasing the shift, the bottom of the conduction band moves up in energy to 0.07 eV above the Fermi level. This system then becomes half-metallic with a band gap in one spin-channel equal to 0.48 eV.

In Fig. 5 we present a different tetragonal displacement involving two symmetrical shifts of 5% of the lattice parameter for two oxygen atoms from LaO and SrO layers in  $La_2SrMn_3O_9$ . For the mixed valence ground state configuration  $Mn^{3+}/Mn^{4+}/Mn^{3+}$  we obtain a half-metallic state. In comparison with the above  $Mn^{4+}/Mn^{3+}$  double unit cell, the band gap has become nearly twice larger, at 0.8 eV. This is due to the higher concentration of  $Mn^{3+}$  atoms in the latter supercell. The results of these two implementations of tetragonal distortions show that if random Jahn-Teller distortions occur,<sup>15</sup> the system can become locally half-metallic.

## VII. PHASE SEPARATION AND CHARGE ORDER IN LSMO

Supercells in the FM regime were also constructed to model both the influence of  $Mn^{4+}$  and  $Mn^{3+}$  ordering on the total energy and the influence of the ordering of the LaO and SrO planes on the Mn charge order. Specifically, supercells of the form  $La_nSrMn_{(n+1)}O_{3(n+1)}$  with  $n = 2, \dots, 7$  and  $La_4Sr_2Mn_6O_{18}$ , and  $La_4Sr_4Mn_8O_{24}$  were studied. Calculations for these systems were in agreement with the results of Fig. 1. Specifically, for  $n$  smaller than 4, the  $La_nSrMn_{(n+1)}O_{3(n+1)}$  systems had an  $Mn^{4+}$  ground state and for  $n$  larger than 4, the mixed valence  $Mn^{4+}/Mn^{3+}$  system became the ground state.

For the mixed valence configuration, we investigated the influence of different distributions of  $Mn^{4+}$  and  $Mn^{3+}$  on the total energy. In particular, we studied different scenarios of distributions of  $Mn^{4+}/Mn^{3+}$  atoms from all  $Mn^{4+}$  (denoted by (444444) in Table III) to all  $Mn^{3+}$  (referred to as (333333) in Table III), using both a six chemical units rigid band model of  $La_{0.83}Sr_{0.17}MnO_3$  and the  $La_5SrMn_6O_{18}$  supercell. In the supercell, the SrO layer was taken to be at the bottom of the cell. The energy differences are small and to emphasize this we write them down in meV. They are nearly equal to the magnitude of magnetic structure energy differences. The distribution 434343 of  $Mn^{4+}$  and  $Mn^{3+}$  valencies was the most favourable energy state at 17% Sr concentration for both the supercell and the rigid band model calculations. A different distribution of the same amount of  $Mn^{4+}$  and  $Mn^{3+}$  atoms denoted by 444333 is about as unfavourable as localizing an extra Mn  $d$  electron, as realized in 334433 scenario, or delocalizing an Mn  $d$  electron as it happens in 443344 scenario. The energy differences between rigid band model calculations and the supercell show that SrO and LaO layers do matter. In the rigid band model we see smaller energy differences upon increasing the amount of  $Mn^{4+}$  cations (only 7 meV separate the 444444 state from the ground state) than upon decreasing the amount of  $Mn^{4+}$  cations (215 meV separate the (333333) state from the ground state). In the supercell approach this trend is not as pronounced and whilst 213 meV separate the 333333 state from the ground state, the 444444 configuration is further away from the ground state, by 27 meV, than in the rigid band model.

The  $La_4Sr_2Mn_6O_{18}$  system, i.e. increasing the Sr concentration to  $\sim 30\%$ , acquires the  $Mn^{4+}$  ground state configuration and is metallic. For this system we have studied the influence of the distribution of SrO and LaO layers on the total energy. The state with the lowest energy was attained by phase separating the SrO layers from the LaO layers, namely the two SrO layers were nearest neighbors. Separating the two SrO layers by one and two LaO layers, respectively, increases respectively the energy of the system by 2 and 5 mRy.

In Fig. 6, we show density of states (DOS) of one of the configurations of  $La_4Sr_2Mn_6O_{18}$ . The configuration is such that we have one  $MnO_2$  plane with  $Mn^{4+}$ , sandwiched between two SrO planes, and all other  $MnO_2$  planes are occupied by  $Mn^{3+}$ . This supercell can be considered as a model of phase separated LSMO which was studied by Koida.<sup>27</sup> It is also of relevance to the  $La_{0.7}Ca_{0.3}MnO_3$  system investigated by Bibes.<sup>23</sup> As can be seen from Fig. 6, this system LSMO is half-metallic. Energetically unfavourable, however, the energy difference between this state and the ground state is reduced to 20 mRy, in comparison with the energy difference between all Mn having the  $Mn^{3+}$  configuration and the ground state (33 mRy). The gap is reduced from 0.68 eV (the scenario with the configuration of  $Mn^{3+}$  for all manganese atoms) to 0.54 eV. Note that this pseudogap is constant for all  $MnO_2$  layers, independently of their valence. None of the supercells had this  $Mn^{3+}$  valence in their ground state configuration. However one could speculate that maybe at the surface  $Mn^{3+}$  could be the stable configuration since the lower coordination would favour the more localised state. More complex supercells, where more Sr layers could phase separate, could plausibly lead to a half-metallic ground state.

The magnetic moment increases from  $2.82 \mu_B$  for Mn sandwiched between two SrO planes (denoted by  $Mn_{SrO-SrO}$ ) to  $2.99 \mu_B$  for  $Mn_{LaO-LaO}$  (Mn sandwiched between two LaO planes) in the  $Mn^{4+}$  configured ground state and from  $3.45 \mu_B$  for  $Mn_{SrO-SrO}$  to  $3.67 \mu_B$  for  $Mn_{LaO-LaO}$  in the half-metallic  $Mn^{3+}$  configuration. We note that the magnetic moments on the oxygen atoms in the SrO layers are dramatically reduced in the vicinity of  $Mn^{3+}$ , namely, a value

TABLE III: Total energy differences (in meV), with respect to the state with the lowest energy, for different distributions of manganese ions, in six units supercell in the rigid band (corresponding to  $\text{La}_{0.83}\text{Sr}_{0.17}\text{MnO}_3$ ) and, in the supercell  $\text{La}_5\text{SrMn}_6\text{O}_{18}$ . For  $\text{La}_5\text{SrMn}_6\text{O}_{18}$  the system is ordered as  $\text{SrO-LaO-LaO-LaO-LaO-LaO}$  and the  $\text{Mn}^{4+}$  or  $\text{Mn}^{3+}$  ions are sandwiched in between.

Scenario	Supercell	Rigid Band Model
444444	27	7
444443	36	–
444434	34	7
444344	48	–
443344	54	41
444343	27	11
434434	45	18
434343	0	0
444333	79	63
334433	104	102
334343	59	52
343343	45	43
333333	213	215

of  $0.01\mu_B$  is obtained, and they have values of 0.15 and  $0.2\mu_B$  in the vicinity of  $\text{Mn}^{3+}/\text{Mn}^{4+}$  and  $\text{Mn}^{4+}$  respectively. The magnetic moments of the O atoms residing in the LaO plane remain small at  $0.05\mu_B$  independently of the Mn valency. In contrast, the O magnetic moments in the  $\text{MnO}_2$  planes are small with values around  $0.05\mu_B$  and do not change much depending on Mn valency except for  $\text{Mn}^{4+}$  at the SrO/LaO interface were an O magnetic moment as large as  $0.1\mu_B$  has been calculated.

Through the study of the  $\text{La}_4\text{Sr}_4\text{Mn}_8\text{O}_{24}$  supercell we model an even further increase of the Sr concentration to 50%. The geometry of the supercell is four La layers separated from the four Sr layers. For this supercell the ground state configuration is all  $\text{Mn}^{4+}$  and this has 31 mRy lower energy than the half-metallic system with mixed valence  $\text{Mn}^{4+}/\text{Mn}^{3+}$  configuration (33333444) and 61 mRy lower than the configuration with all  $\text{Mn}^{3+}$ . The magnetic moments, which are smaller than for 30% Sr, are increasing, as is also the case for 30% Sr, from  $2.71\mu_B$  for  $\text{Mn}_{\text{SrO-SrO}}$  to  $3.05\mu_B$  for  $\text{Mn}_{\text{LaO-LaO}}$  in the  $\text{Mn}^{4+}$  configured ground state, and from  $3.56\mu_B$  for  $\text{Mn}_{\text{SrO-SrO}}$  to  $3.61\mu_B$  for  $\text{Mn}_{\text{LaO-LaO}}$  in the half-metallic  $\text{Mn}^{3+}$  configuration. For the latter, more localised configuration, we note a large sensitivity of the magnetic moments of the oxygen atoms from the LaO layers to the presence of the SrO/LaO interface. At the interface the O magnetic moment of the LaO layer practically disappears. Away from the interface, this moment is  $0.1\mu_B$  and remains constant in these LaO layers. In the SrO layers the O magnetic moment is slightly larger, at  $0.13\mu_B$ , and remains constant in all SrO layers including the interface one.

### VIII. CONCLUSIONS

We have found that the ground state configuration of LSMO consists of manganese in the 4+ valence configuration. For Sr concentrations less than 20%, a mixed valence  $\text{Mn}^{4+}/\text{Mn}^{3+}$  ground state was obtained, whilst for concentrations in excess of 20% a  $\text{Mn}^{4+}$  ground state was obtained. Also, a close competition between FM and AF-A  $\text{Mn}^{4+}$  states was seen with a crossover from FM to AF-A  $\text{Mn}^{4+}$  around 35% Sr concentration. The  $\text{Mn}^{4+}$  ground state has marginal spin polarization at the Fermi level. We found, however, that the  $\text{Mn}^{3+}$  valency was not that energetically unfavourable and that small increases in the lattice parameter would lead to the occurrence of  $\text{Mn}^{3+}$  in a mixed valence  $\text{Mn}^{4+}/\text{Mn}^{3+}$  state. Likewise, elongations of the  $\text{MnO}_6$  octahedra lead to the formation of  $\text{Mn}^{3+}$  valence atoms. With the appearance of  $\text{Mn}^{3+}$  ions a half-metallic state is obtained. Furthermore, in the mixed valence state we found that the total energy is minimized by an ordered array of  $\text{Mn}^{4+}$  and  $\text{Mn}^{3+}$   $\text{MnO}_2$  planes. The relation of this finding to the observed charge-ordered stripes<sup>33</sup> will be the topic of a further study.

As the Sr doping increases, the  $\text{Mn}^{4+}$  state becomes more and more favoured with respect to the  $\text{Mn}^{3+}$ . The Sr doping results in one more valence band electron which is obtained from delocalizing a  $\text{Mn}^{3+} e_g$  state. In other words, Sr hole doping favours band formation instead of localization.

Finally, for  $\text{La}_{0.7}\text{Sr}_{0.3}\text{MnO}_3$ , of huge relevance to spintronics applications, we suggest the following scenario to explain the half-metallic properties. Whilst in  $\text{La}_{0.7}\text{Sr}_{0.3}\text{MnO}_3$ , from x-ray results, every Mn-O bondlength is the same at  $1.949\text{ \AA}$ ,<sup>26</sup> the bondlengths of Mn-O in distorted LMO change from  $1.907\text{ \AA}$  to  $2.179\text{ \AA}$ , depending on direction. It seems however, based on pulsed-neutron diffraction measurements,<sup>15</sup> that the Jahn-Teller distortion is

still present in LSMO and could therefore, according to our analysis, lead to the formation of  $Mn^{3+}$  ions, which would be sufficient to give rise to a half-metallic state.

### Acknowledgements

G.B. was supported by the EU-funded Research Training Network: "Computational Magnetoelectronics" (HPRN-CT-2000-00143).

---

<sup>1</sup> M. Bowen, M. Bibes, A. Barthelemy, J.-P. Contour, A. Anane, Y. Lemaitre, and A. Fert, *App. Phys. Lett.* **82**, 233 (2003).  
<sup>2</sup> W.E. Pickett, D.J. Singh, *JMMM* **172**, 237 (1997).  
<sup>3</sup> D.J. Singh, W.E. Pickett, *Phys. Rev. B* **57**, 88 (1998).  
<sup>4</sup> D.J. Singh, W.E. Pickett, *J. App. Phys.* **83**, 7354 (1998).  
<sup>5</sup> E.A. Livesay, R. N. West, S.B. Dugdale, G. Santi and T. Jarlborg, *J. Phys. Cond. Matt.* **11**, L2711 (1999).  
<sup>6</sup> B. Nadgorny, I. I. Mazin, M. Osofsky, R. J. Soulen, Jr., P. Broussard, R. M. Stroud, D. J. Singh, V. G. Harris, A. Arsenov and Y. Mukovskii, *Phys. Rev. B* **63**, 184433 (2001).  
<sup>7</sup> I.I. Mazin, *Phys. Rev. Lett.* **83**, 1427 (1999).  
<sup>8</sup> J. M. D. Coey, M. Viret, *Adv. Phys.* **48**, 167 (1999).  
<sup>9</sup> Y. Tokura, Y. Tamioka, *JMMM* **200**, 1 (1999).  
<sup>10</sup> M. Dzero, L. P. Gor'kov, and V. Z. Kresin, *cond-mat/0208005*.  
<sup>11</sup> B. Michaelis and A. J. Millis, *cond-mat/0212573*.  
<sup>12</sup> J. Hemberger, A. Krimmel, T. Kurz, H.-A. Krug von Nidda, V. Yu. Ivanov, A. A. Mukhin, A. M. Balbashov, A. Loidl, *cond-mat/0204269*.  
<sup>13</sup> Ryo Maezono, Sumio Ishihara, and Naoto Nagaosa, *Phys. Rev. B* **58**, 11583 (1998).  
<sup>14</sup> Peter Majewski, Lars Epple, Michael Rozumek, Heike Schluckwerder, and Fritz Aldinger, *J. Matte. Res. B* **15**, 1161 (2000).  
<sup>15</sup> Despina Louca and T. Egami, *Phys. Rev. B* **59**, 6193 (1999).  
<sup>16</sup> J. L. Cohn, J. J. Neumeier, C. P. Popoviciu, K. J. McClellan, Th. Leventouri, *Phys. Rev. B* **56**, R8495 (1997).  
<sup>17</sup> T. Saitoh, A. E. Bocquet, T. Mizokawa, H. Namatame, A. Fujimori, M. Abbate, Y. Takeda and M. Takano, *Phys. Rev. B* **51**, 13942 (1995).  
<sup>18</sup> G. Subias, J. Garcia, M. G. Proietti, and J. Blasco, *Phys. Rev. B* **56**, 8183 (1997).  
<sup>19</sup> J. -H. Park, E. Vescovo, H. -J. Kim, C. Kwon, R. Ramesh and T. Venkatesan *Nature* **392**, 794 (1998).  
<sup>20</sup> W.M. Temmerman, A. Svane, Z. Szotek and H. Winter, in *Electronic Density Functional Theory: Recent Progress and New Directions*, J.F. Dobson, G. Vignale, and M.P. Das (eds.), Plenum Press, New York and London, 1998.  
<sup>21</sup> R. Tyer, W. M. Temmerman, Z. Szotek, G. Banach, A. Svane, L. Petit, G. A. Gehring, *cond-mat/0303602*.  
<sup>22</sup> J.P. Perdew and A. Zunger, *Phys. Rev. B* **23**, 5048 (1981).  
<sup>23</sup> M. Bibes, Ll. Balcells, S. Valencia, and J. Fontcuberta, M. Wojcik, E. Jedryka, and S. Nadolski, *Phys. Rev. Lett.* **87**, 067210 (2001).  
<sup>24</sup> B. C. Haubak, H. Fjelvag, N. Sakai, *J. Solid State Chem.* **124**, 43 (1996).  
<sup>25</sup> P.D. Baattle, T.C. Gibb, C.W. Jones, *J. Solid State Chem.* **74**, 60 (1988).  
<sup>26</sup> S. J. Hibble, S.P. Cooper, A.C. Hannon, I.D. Fawcett and M. Greenblatt, *J.Phys.: Condens. Matter* **11**, 9221 (1999).  
<sup>27</sup> T. Koida, M. Lippmaa, T. Fukumura, K. Itaka, Y. Matsumoto, M. Kawasaki, and H. Koinuma, *Phys. Rev. B* **66**, 144418 (2000).  
<sup>28</sup> O.K. Andersen, *Phys. Rev. B* **12**, 3060 (1975).  
<sup>29</sup> O.K. Andersen and O. Jepsen, *Phys. Rev. Lett.* **53**, 2571 (1984).  
<sup>30</sup> W.R.L. Lambrecht and O.K. Andersen, *Phys. Rev. B* **34**, 2439 (1986).  
<sup>31</sup> I. Loa, P. Adler, A. Grzechnik, K. Syassen, U. Schwarz, M. Hanfland, G.Kh. Rozenberg, P. Gorodetsky, and M.P. Pasternak, *Phys. Rev. Lett.* **87**, 125501 (2001).  
<sup>32</sup> Warren E. Pickett and David J. Singh, *Phys. Rev. B* **53**, 1146 (1996).  
<sup>33</sup> P. Littlewood, *Nature* **399**, 529 (1999).

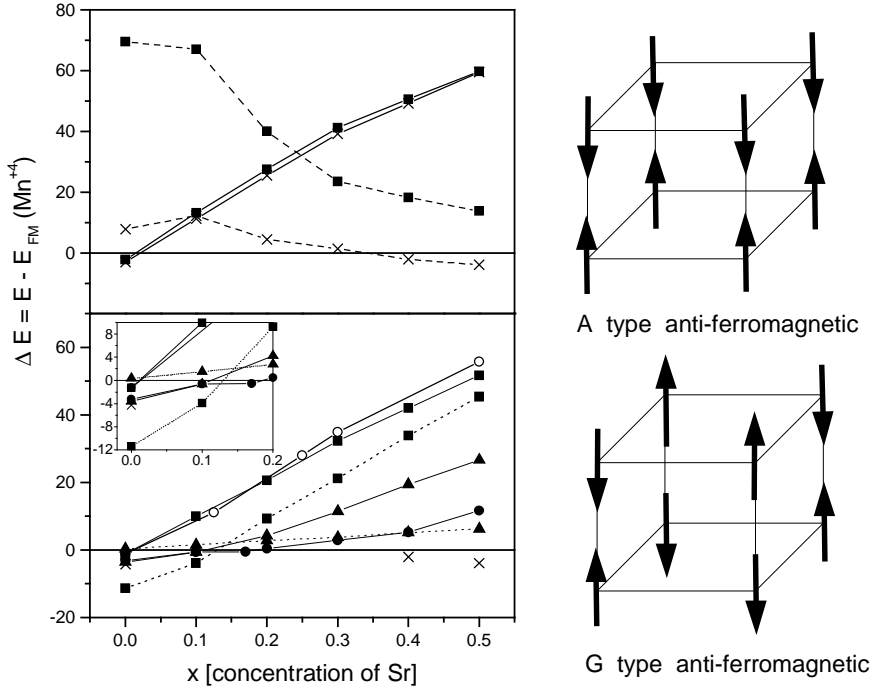


FIG. 1: Left: Energy phase diagram LMO – LSMO in the cubic structure with the lattice constant of 7.32 a.u.. The energy for all the systems is with respect to the energy of FM system with  $Mn^{4+}$ . Top: AF-A – crosses with solid and dashed lines for  $Mn^{3+}$  and  $Mn^{4+}$  respectively; AF-G – squares with solid and dashed lines for  $Mn^{3+}$  and  $Mn^{4+}$ , respectively. Bottom, FM:  $Mn^{3+}$  - squares with solid line;  $Mn^{4+}/Mn^{3+}$  supercell – solid circles with solid line;  $Mn^{3+}/Mn^{4+}/Mn^{3+}$  supercell - triangles with solid line;  $Mn^{4+}/Mn^{3+}/Mn^{4+}$  supercell – triangles with dashed line;  $Mn^{3+}$  for the lattice constant of 7.434 – squares with dashed line;  $Mn^{3+}$  for appropriate supercell – open circles with solid line. The crosses on their own show AF-A ground state for LSMO. Right: Schematic views of the AF-A and AF-G structures.

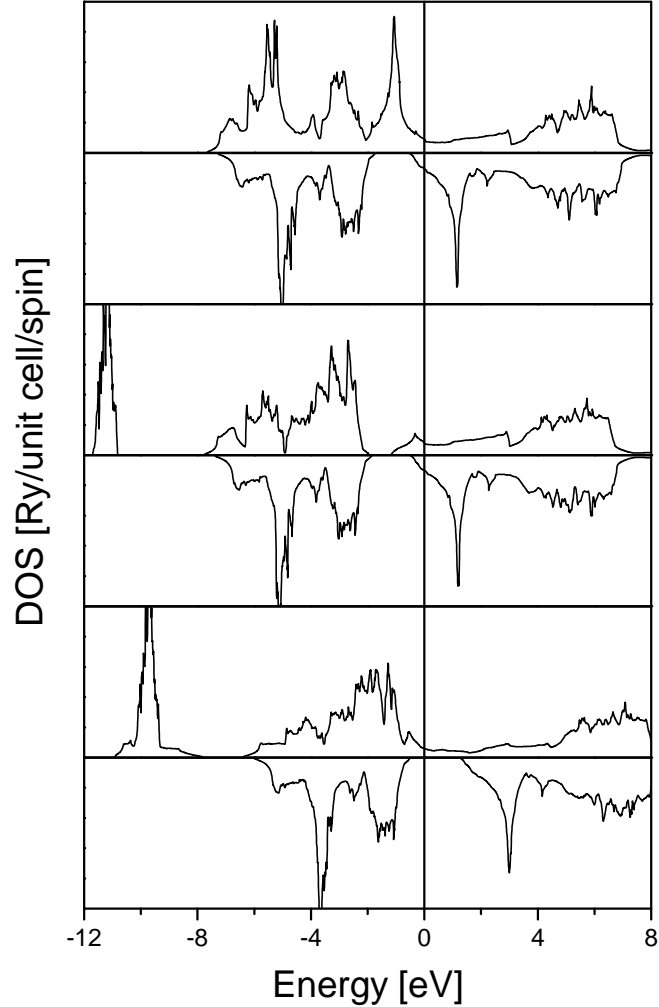


FIG. 2: Density of states for FM  $\text{La}_{0.7}\text{Sr}_{0.3}\text{MnO}_3$  from rigid band model for minority and majority spin channels with respect to the Fermi energy. Displayed are: LSD calculation (top), SIC–LSD calculation for the ground state of three localised  $t_{2g}$  electrons (centre) and SIC–LSD calculation for four localised electrons ( $3t_{2g} + e_g(3z^2 - r^2)$ ) (bottom).

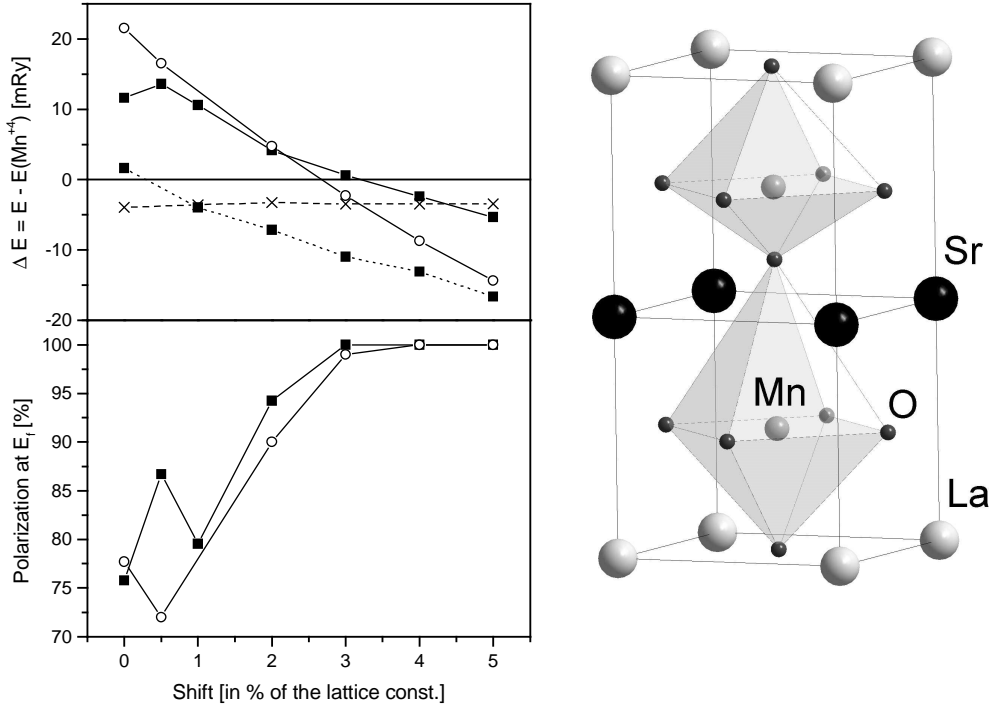


FIG. 3: Left: In the top panel the energy difference for the FM system in the  $\text{Mn}^{4+}/\text{Mn}^{3+}$  mixed valence state: squares with solid line - rigid band model (for  $x=0.5$ ); open circles - supercell model ( $\text{LaSrMn}_2\text{O}_6$ ); squares with dotted line - rigid band model (for  $x=0.3$ ), and AF-A with  $\text{Mn}^{4+}$  - crosses with dashed line. All energies are with respect to the energy of the FM system with  $\text{Mn}^{4+}$ . In the bottom panel: polarisation of electrons at the Fermi level: squares - from rigid band model (for  $x=0.5$ ) and open circles for supercell model ( $\text{LaSrMn}_2\text{O}_6$ ). Right: Schematic view of the unit cell.

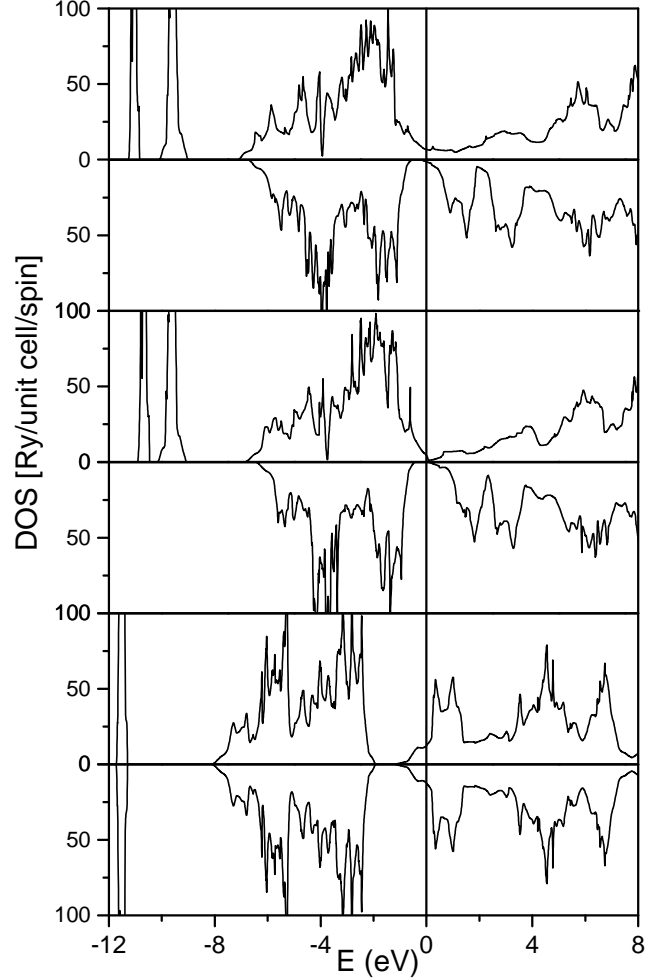


FIG. 4: DOS for  $\text{LaSrMn}_2\text{O}_6$  with mixed valence  $\text{Mn}^{4+}/\text{Mn}^{3+}$  configurations for minority and majority spin channel: is metallic without tetragonal shift for oxygen atom (top), is half-metallic with a tetragonal shift applied to the oxygen atom of 0.04 of the lattice constant (centre). In the bottom panel is the DOS for the antiferromagnetic ground state of  $\text{Mn}^{4+}$  without tetragonal shift.

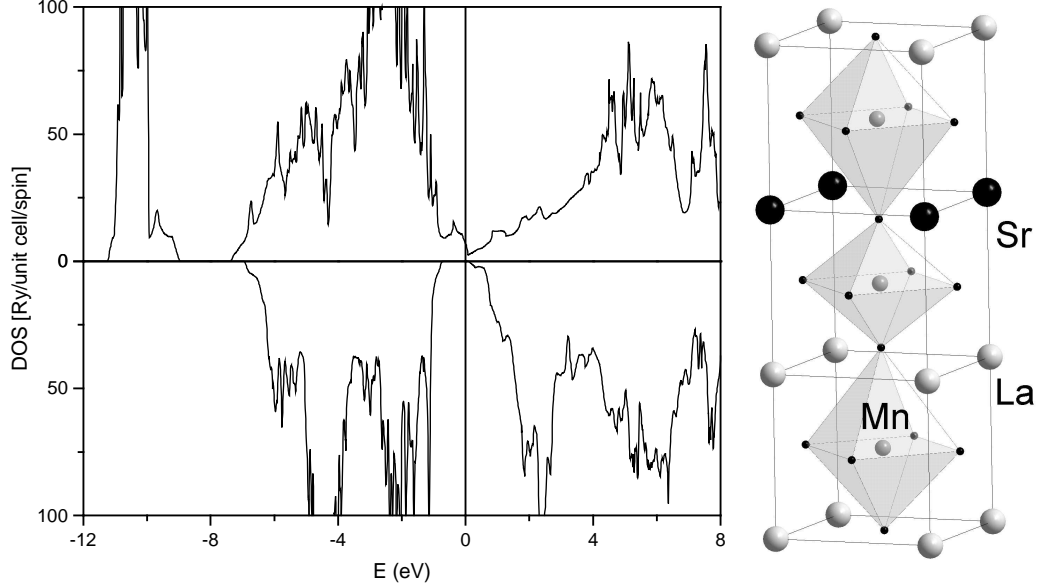


FIG. 5: Left: DOS, in minority and majority spin channels, for  $\text{La}_2\text{SrMn}_3\text{O}_9$  with symmetrically shifted (by 0.05 of lattice constant) oxygen atoms for the mixed  $\text{Mn}^{3+}/\text{Mn}^{4+}/\text{Mn}^{3+}$  configuration. Right: Schematic view of the unit cell.

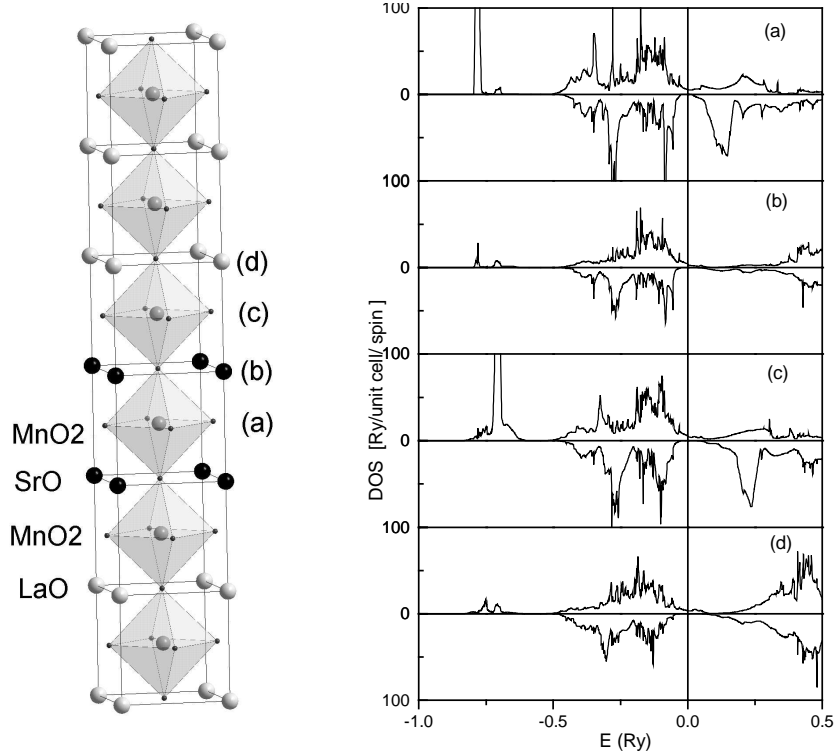


FIG. 6: Local DOS for a supercell  $\text{La}_4\text{Sr}_2\text{Mn}_6\text{O}_{18}$  (right). The configuration is (a) one  $\text{MnO}_2$  layer of  $\text{Mn}^{4+}$  sandwiched between the  $\text{SrO}$  layers (marked as black balls) and  $\text{Mn}^{3+}$  in all other  $\text{MnO}_2$  planes. Here (b) refers to  $\text{SrO}$  plane, (c) to  $\text{MnO}_2$  plane, and (d) to  $\text{LaO}$  plane. The left-hand-side picture shows the structure.